Optics Letters

Second-harmonic computer-generated holographic imaging through monolithic lithium niobate crystal by femtosecond laser micromachining

Bing Zhu,† Haigang Liu,† Yi'an Liu, Xiongshuo Yan, Yuping Chen,* and Xianfeng Chen

State Key Laboratory of Advanced Optical Communication Systems and Networks, School of Physics and Astronomy, Shanghai Jiao Tong University, 800 Dongchuan Road, Shanghai 200240, China
**Corresponding author: ypchen@sjtu.edu.cn*

Received 7 April 2020; revised 23 May 2020; accepted 26 June 2020; posted 29 June 2020 (Doc. ID 394162); published 17 July 2020

The computer-generated holography technique is a powerful tool for three-dimensional display, beam shaping, optical tweezers, ultrashort pulse laser parallel processing, and optical encryption. We have realized nonlinear holography in ferroelectric crystals by utilizing spatial light modulators in our previous works. Here, we demonstrate an improved method to realize second-harmonic (SH) holographic imaging through a monolithic lithium niobate crystal based on binary computer-generated holograms (CGHs). The CGH patterns were encoded with the detour phase method and fabricated by femtosecond laser micromachining. By the use of the birefringence phase-matching process in the longitudinal direction, bright nonlinear holograms can be obtained in the far-field. The realization of SH holography through monolithic crystal opens wide possibilities in the field of high power laser nonlinear holographic imaging.

https://doi.org/10.1364/OL.394162

Optical holography is a wavefront reconstruction technique that records and reconstructs the amplitude and phase of a light wave from an illuminated object. It was first proposed and realized by Dennis Gabor in 1948 [1]. With the development of the information age, computer technology and holography have been integrated more closely and have led to the emergence of the computer-generated holograms (CGHs) [2]. The CGH technology can model the interference recording progress on a computer without performing experiments by the use of an optical system. It has been widely used in various fields, such as three-dimensional (3D) display [3–5], image projection [6], beam shaping [7,8], optical tweezers [9–11], ultrashort pulse laser parallel processing [12,13], and optical encryption [14,15]. Nowadays, computer-generated holographic imaging has been realized in various ways, including metamaterials [16–18], spatial light modulators (SLMs) [19–22], and diffractive optical elements (DOEs) [23–27]. However, these ways achieved holographic imaging in the linear optics and had some limitations when applied to the nonlinear field.

Nonlinear frequency conversion with the quadratic nonlinear crystals is an important method to generate coherent radiations [28]. In recent years, the combination of nonlinear frequency conversion and wavefront shaping has been widely studied [29–32]. At present, there are two main methods to realize nonlinear wavefront shaping. One is to generate the second-harmonic (SH) wave from the nonlinear crystal first and then conduct the wavefront shaping through SLMs. We have used this method to realize dynamic SH wavefront modulation in our previous work [33]. Due to the limitation of SLMs, this method increases the complexity of the system and cannot withstand high power laser irradiation. Another way is integrating the wavefront shaping process within the nonlinear materials by the use of nonlinear photonic crystals (NPCs) [34]. By using the electric-field poling technique [30–32] or femtosecond laser micromachining [35–38], the second-order nonlinear coefficient $\chi^{(2)}$ of the NPC can be spatially modulated for wavefront shaping. In our previous research, we have realized the efficient two-dimensional (2D) nonlinear wavefront shaping in amplitude-type NPCs by femtosecond laser micromachining [8]. Nowadays, nonlinear computer-generated holographic imaging has been attracting extensive research interest.

In this Letter, we demonstrate a general approach to realize the nonlinear computer-generated holographic imaging in monolithic lithium niobate ($LiNbO_3$) crystal. We have chosen two specific original images: "SJTU" and the Shanghai Jiao Tong University (SJTU) logo for experiments. We encoded these images with the detour phase method. The calculated CGH patterns were fabricated in $LiNbO_3$ with 0 or +1 binary modulation of quadratic susceptibility by femtosecond laser micromachining. The modulated $LiNbO_3$ crystal was cut for a specific angle between the optical axis and the z axis, where the phase-matching condition is fulfilled through birefringence

phase matching (BPM) in the longitudinal direction. By sending a nanosecond laser of 1064 nm wavelength to the fabricated CGH, the bright SH holographic imaging can be achieved in the far-field.

The process of creating a CGH can be broken down into three separate parts. First is the computational part, which involves the calculation of the complex fields in the hologram plane with discrete sampling points by a fast Fourier transform (FFT) algorithm. The second part of the process is the encoding part, which involves the choice of a suitable encoding method for the complex fields in the hologram plane. The third part of the process is the fabrication part, which involves the transfer of the encoded representation of the complex fields to a transparency object. Because the computation part has been developed into a universal algorithm in Ref. [39], we will not elaborate here. The following content of this Letter will illustrate the encoding and fabrication part.

The choice of an encoding method is often influenced by the properties of the fabrication device that will be used, so the second and third parts of the problem are not entirely independent. Since we use the femtosecond laser to modulate the crystal with either an entirely positive or an erased zero quadratic susceptibility throughout the interaction region [38] in the fabrication part, the binary CGH was chosen to generate in our experiments, and then the most appropriate encoding method is the detour phase method [40]. In the detour phase method, an elementary cell is allocated for reproducing the amplitude and phase of each sampling point of the CGH. The modulus of the complex number is represented by the size of the opening (aperture) in the cell, and the phase is represented by the position of the opening within the cell.

The schematic illustration of the holographic imaging encoding process is shown in Fig. 1. We used a binary image with the dimensions of $M \times N$ pixels as the object and conducted the FFT process with the software of MATLAB [41]. A 2D complex value matrix can be achieved as follows:

$$F_{mn} = A_{mn} \cdot \exp(j \cdot \Phi_{mn}), \quad m \text{ (or } n) = 1, 2, \cdots, M \text{ (or } N), \tag{1}$$

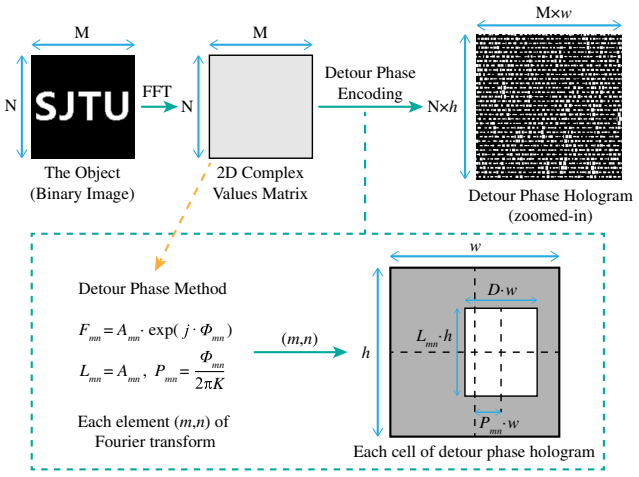

Fig. 1. Schematic illustration of the holographic imaging encoding process. The lower part of the diagram shows the principle of the binary detour phase method for representing the hologram. FFT, fast Fourier transform.

where A_{mn} and Φ_{mn} are the amplitude and phase of the complex value F_{mn}, respectively. After computing Fourier elements of the desired binary image (the object), each of these elements is represented by an opaque cell with dimensions of $w \times h$. Based on the detour phase method [40], each cell has a rectangular transparent aperture; the width of the rectangular aperture $D \cdot w$ is fixed, the height $L_{mn} \cdot h$ is proportional to the amplitude A_{mn} of different points (m, n), and the distance from the center of the opaque cell $P_{mn} \cdot w$ is proportional to the phase Φ_{mn} of different points (m, n). The specific relationship is shown as follows:

$$\begin{cases} L_{mn} = A_{mn} \\ P_{mn} = \frac{\Phi_{mn}}{2\pi K} \end{cases}. \tag{2}$$

The maximum value of A_{mn} is normalized to 1. The parameter K determines the effective carrier frequency of the binary hologram. In our experiments, we have chosen the following parameters: $D = 0.5$, $K = 1$. This coding process is carried out for all the cells in the hologram with the software of MATLAB.

After the computation part, we fabricated the detour phase holograms in $LiNbO_3$ crystal with femtosecond laser pulses, as shown in Fig. 2. The hologram pattern has been fabricated in a 5 mol.% MgO-doped $LiNbO_3$ crystal [42], which has the dimensions of 10 mm(x) × 10 mm(y) × 1 mm(z). In addition, It was cut for a specific angle of $\theta = 75°$ between the optical axis (c axis) and the z axis of the crystal. We used a compact ytterbium-doped diode-pumped ultrafast amplified laser as a laser source, which delivered linearly polarized pulses with a duration of 500 fs. The center wavelength is 1030 nm, and the repetition rate is 1 kHz. An objective lens with a numerical aperture of 0.50 (RMS20X-PF, Olympus) was applied to focus the laser pulses. The crystal sample was mounted on a computer-controlled XYZ translation piezo-stage with 0.1 μm resolution. Controlling by the computer program, the crystal sample was moved step by step and irradiated by the focused femtosecond laser pulses. The irradiated dots became "black" by selectively erasing the ferroelectric domain, while the unirradiated dots remained "blue." A magnified illustration of the geometric specific pattern with 0 or +1 binary modulation of the quadratic

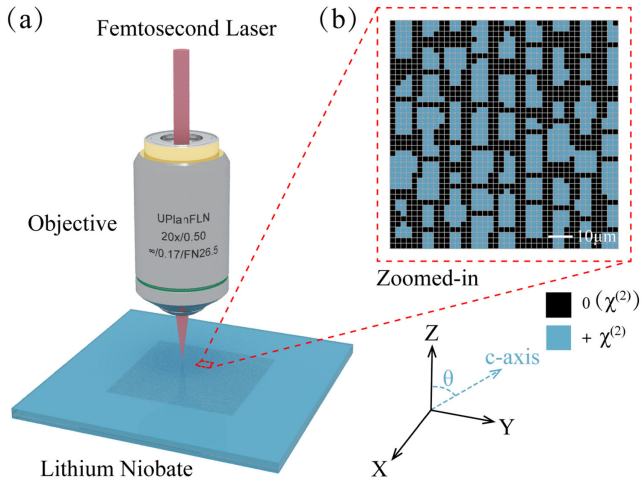

Fig. 2. (a) Schematic illustration of the CGH pattern fabrication process using femtosecond laser micromachining. (b) The zoomed-in geometric specific pattern with 0 or +1 binary modulation of the quadratic nonlinear susceptibility $\chi^{(2)}$ in lithium niobate. The crystal was cut for a specific angle between the c axis and z axis.

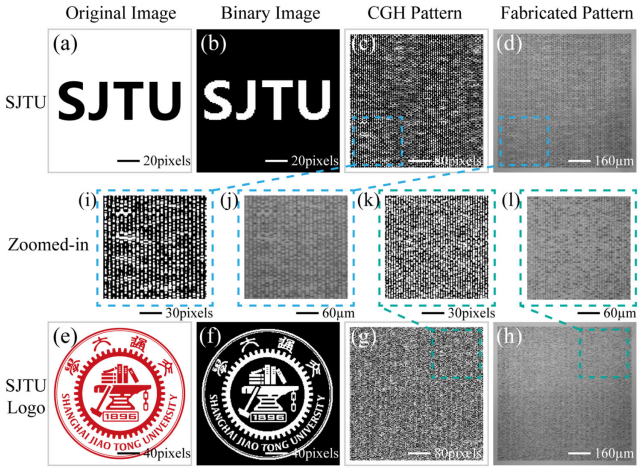

Fig. 3. Comparison between original images, binary images, calculated CGH patterns, and fabricated patterns of two specific images: (a)–(d) "SJTU" and (e)–(h) SJTU logo. (i)–(l) show the zoomed-in images.

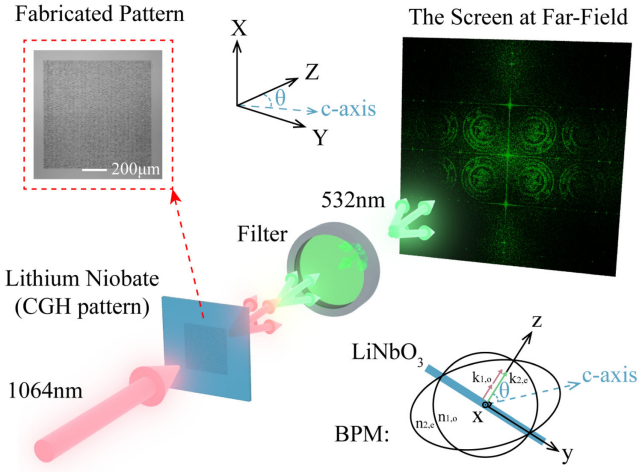

Fig. 4. Schematic illustration of the SH holographic imaging setup in lithium niobate ($LiNbO_3$) crystal pumped by the Nd:YAG laser with 10.5 ns pulse duration at a 1 kHz repetition rate at 1064 nm. The screen in the far-field is the simulation result of the SJTU logo SH holographic imaging. The filter is used to separate the FF and SH beams. The lower right section is the schematic illustration of the BPM process, where $\vec{k}_1$ represents the wave vector of the FF beam and $\vec{k}_2$ represents the wave vector of the SH beam, n_1 represents the refractive index of the FF beam, and n_2 represents the refractive index of the SH beam. Subscripts "o" and "e" represent the ordinary and extraordinary polarized light, respectively.

nonlinear susceptibility $\chi^{(2)}$ in $LiNbO_3$ is shown in Fig. 2(b). The physical mechanism of the ferroelectric domain erasing process can be understood in that the crystallinity is reduced through laser irradiation [38]. It should be noted that the refractive index of the crystal was changed of 2.5×10^{-3}, which was calculated by a diffraction method [43]. We fabricated the specific hologram pattern with 512×512 pixels, where each pixel has a size approximately at 2 μm × 2 μm by the scanning process of the femtosecond laser pulses. The chirped pulses were focused 30 μm beneath the front surface of the crystal with the incident energy of 0.9 μJ per pulse. It was first scanned in x direction step by step and then moved to the next pixel by moving in the $+y$ direction. The translation speed of the stage is 280 μm/s. The odd pixels and even pixels were all scanned in the same $+x$ direction. It is worth mentioning that it took about 3.5 h to fabricated the 512×512 pixels binary phase hologram in $LiNbO_3$ with femtosecond laser pulses.

For demonstrating nonlinear holographic imaging, we have used two specific original images: "SJTU" and the SJTU logo for experiments. The comparisons between the original images, binary images, calculated CGH patterns, and fabricated patterns of these two specific images are shown in Fig. 3. We have converted the original images to the binary images for the convenience of encoding the images with the detour phase method. It is worth mentioning that the binary images of "SJTU" and the SJTU logo have the dimensions of 128×128 pixels and 256×256 pixels, respectively. The CGH patterns of these two images have been enlarged to the dimensions of 512×512 pixels for the convenience of the fabrication process. The two fabricated patterns [Figs. 3(d) and 3(h)] and their zoomed-in images [Figs. 3(j) and 3(l)] show the excellent quality of the femtosecond laser fabrication process.

The schematic illustration of the SH holographic imaging setup is shown in Fig. 4. An Nd:YAG laser producing 10.5 ns pulses at a 1 kHz repetition rate at a wavelength of 1064 nm has been used as the fundamental frequency (FF) source. The ordinary polarized laser beam was irradiated on the center of the fabricated hologram pattern in the crystal, which created a waist radius of approximately 500 μm. The polarization axis of the incident ordinary polarized fundamental wave is parallel to the x direction, and an extraordinary polarized SH beam at the wavelength of 532 nm was generated through the crystal. We have used a filter (TF1, Thorlabs) to separate the FF and SH beams. Also, the illustration shows the fabricated pattern of the SJTU logo image and the transverse setting in which the experiment took place. Numerical simulation was performed on a screen at far-field based on the split-step Fourier method with the software of MATLAB. The $LiNbO_3$ crystal was cut for the Type I (oo-e) phase-matching process based on the BPM [44] theory. Hence, the longitudinal part of the vectorial phase-matching condition was fulfilled, and efficient nonlinear harmonic holographic imaging can be obtained at the far-field. The output SH patterns were projected onto a white screen, which was put 100 cm behind the crystal, and then recorded by a camera.

Figure 5 presents a comparison between the binary images, SH holography imaging simulation results, and experiment results of two specific images: "SJTU" and the SJTU logo. The results show high correlation values between simulations and experiments of the generated holography images: "SJTU" (90%) and the SJTU logo (86%) [45]. In our experiment, the intensity of the fundamental input light is about 300 mW, and the generated total SH intensity is 31.5 μW. The measured normalized conversion efficiency η_{nor} can be calculated by the formula as follows:

$$\eta_{\mathrm{nor}} = \frac{P_{2\omega}}{P_{\omega}^{2} \cdot L^{2}}, \tag{3}$$

where P_{ω} and $P_{2\omega}$ are the powers of the fundamental and harmonic, respectively, and L is the length over which the light beams propagate in the crystal [46]. The normalized conversion

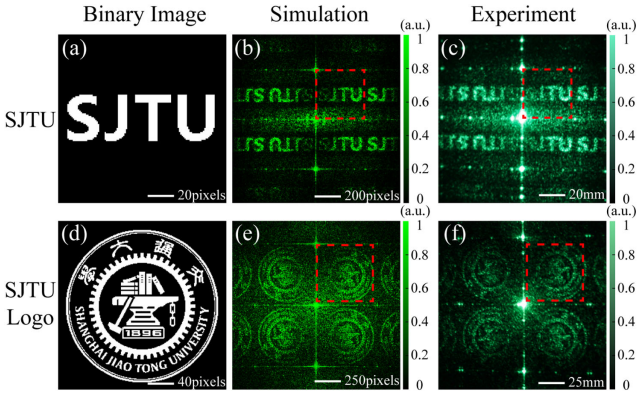

Fig. 5. Comparison between binary images, SH holographic imaging simulation results, and experiment results of two specific images: (a)–(c) "SJTU" and (d)–(f) SJTU logo. The color bars indicate the relative light intensity. (The white regions mean the intensities are beyond the color bars.)

efficiency in our experiment is 3.5% $W^{-1}cm^{-2}$, with the 1 mm thick crystal. The SH diffraction efficiency in our experiments is about 2.8%, and it can be improved by optimizing the encoding algorithms and the fabricated CGH pattern quality [47].

In conclusion, we have demonstrated the realization of the SH holographic imaging in a monolithic lithium niobite crystal by femtosecond laser micromachining. Based on the detour phase method, arbitrary binary images can be encoded to generate hologram patterns. In the future, the combination of optimized encoding algorithms and femtosecond laser fabrication processes can be used to improve the holography quality and the nonlinear harmonic conversion efficiency. The ability to convert the frequency of light and generate holographic imaging simultaneously in a monolithic ferroelectric crystal will be useful for all-optical 3D displays and high power laser nonlinear holographic imaging fields.

Funding. National Natural Science Foundation of China (11574208, 91950107); National Key Research and Development Program of China (2017YFA0303700); Shanghai Jiao Tong University (IPP18053, T072PRP34006).

Disclosures. The authors declare no conflicts of interest.

[†]These authors contributed equally to this Letter.

REFERENCES

1. D. Gabor, Nature **161**, 777 (1948).
2. B. R. Brown and A. W. Lohmann, Appl. Opt. **5**, 967 (1966).
3. R. G. Dorsch, A. W. Lohmann, and S. Sinzinger, Appl. Opt. **33**, 869 (1994).
4. L. Huang, X. Chen, H. Mühlenbernd, H. Zhang, S. Chen, B. Bai, Q. Tan, G. Jin, K.-W. Cheah, C.-W. Qiu, J. Li, T. Zentgraf, and S. Zhang, Nat. Commun. **4**, 2808 (2013).
5. R. Kang, J. Liu, G. Xue, X. Li, D. Pi, and Y. Wang, Opt. Express **27**, 14369 (2019).
6. M. Meem, A. Majumder, and R. Menon, Appl. Opt. **59**, 38 (2020).
7. M. Manousidaki, D. G. Papazoglou, M. Farsari, and S. Tzortzakis, Opt. Lett. **45**, 85 (2020).
8. B. Zhu, H. Liu, Y. Chen, and X. Chen, Opt. Lett. **45**, 220 (2020).
9. J. E. Curtis, B. A. Koss, and D. G. Grier, Opt. Commun. **207**, 169 (2002).
10. D. G. Grier and Y. Roichman, Appl. Opt. **45**, 880 (2006).
11. I. Shishkin, H. Markovich, Y. Roichman, and P. Ginzburg, Micromachines **11**, 90 (2020).
12. A. Gillner, P. Gretzki, and L. Büsing, Proc. SPIE **9740**, 117 (2016).
13. S. Ji, L. Yang, Y. Hu, J. Ni, W. Du, J. Li, G. Zhao, D. Wu, and J. Chu, Small **13**, 1701190 (2017).
14. B. Javidi and T. Nomura, Opt. Lett. **25**, 28 (2000).
15. X. Fang, H. Ren, and M. Gu, Nat. Photonics **14**, 102 (2019).
16. A. C. Overvig, S. Shrestha, S. C. Malek, M. Lu, A. Stein, C. Zheng, and N. Yu, Light Sci. Appl. **8**, 92 (2019).
17. Y. Hu, L. Li, Y. Wang, M. Meng, L. Jin, X. Luo, Y. Chen, X. Li, S. Xiao, H. Wang, Y. Luo, C.-W. Qiu, and H. Duan, Nano Lett. **20**, 994 (2019).
18. C. Min, Y. Zhang, X. Yuan, W. Song, S. Zheng, Z. Xie, and Y. Fu, Chin. Opt. Lett. **17**, 062402 (2019).
19. G. Makey, Ö. Yavuz, D. K. Kesim, A. Turnali, P. Elahi, S. Ilday, O. Tokel, and F. Ö. Ilday, Nat. Photonics **13**, 251 (2019).
20. Y. Qi, C. Chang, and J. Xia, Opt. Express **24**, 30368 (2016).
21. G. Makey, M. S. El-Daher, and K. Al-Shufi, Appl. Opt. **51**, 7877 (2012).
22. S. J. Huang, X. J. Liu, S. Z. Wang, and X. Jiang, Proc. SPIE **7513**, 379 (2009).
23. J. Wang, L. Liu, A. Cao, H. Pang, C. Xu, Q. Mu, J. Chen, L. Shi, and Q. Deng, Micromachines **9**, 508 (2018).
24. R. Berlich, D. Richter, M. Richardson, and S. Nolte, Opt. Lett. **41**, 1752 (2016).
25. F. J. Salgado-Remacha, L. M. Sanchez-Brea, and E. Bernabeu, J. Lightwave Technol. **29**, 850 (2011).
26. Y. Li, Y. Dou, R. An, H. Yang, and Q. Gong, Opt. Express **13**, 2433 (2005).
27. Y. Li, H. Jiang, H. Yang, and Q. Gong, Chin. Opt. Lett. **3**, S200 (2005).
28. P. A. Franken, A. E. Hill, C. W. Peters, and G. Weinreich, Phys. Rev. Lett. **7**, 118 (1961).
29. X. Hu, Y. Zhang, and S. Zhu, Adv. Mater. **32**, 1903775 (2019).
30. B. Yang, X.-H. Hong, R.-E. Lu, Y.-Y. Yue, C. Zhang, Y.-Q. Qin, and Y.-Y. Zhu, Opt. Lett. **41**, 2927 (2016).
31. X.-H. Hong, B. Yang, C. Zhang, Y.-Q. Qin, and Y.-Y. Zhu, Phys. Rev. Lett. **113**, 163902 (2014).
32. A. Shapira, I. Juwiler, and A. Arie, Opt. Lett. **36**, 3015 (2011).
33. H. Liu, X. Zhao, H. Li, Y. Zheng, and X. Chen, Opt. Lett. **43**, 3236 (2018).
34. V. Berger, Phys. Rev. Lett. **81**, 4136 (1998).
35. D. Wei, C. Wang, X. Xu, H. Wang, Y. Hu, P. Chen, J. Li, Y. Zhu, C. Xin, X. Hu, Y. Zhang, D. Wu, J. Chu, S. Zhu, and M. Xiao, Nat. Commun. **10**, 4193 (2019).
36. S. Liu, K. Switkowski, C. Xu, J. Tian, B. Wang, P. Lu, W. Krolikowski, and Y. Sheng, Nat. Commun. **10**, 3208 (2019).
37. T. Xu, K. Switkowski, X. Chen, S. Liu, K. Koynov, H. Yu, H. Zhang, J. Wang, Y. Sheng, and W. Krolikowski, Nat. Photonics **12**, 591 (2018).
38. D. Wei, C. Wang, H. Wang, X. Hu, D. Wei, X. Fang, Y. Zhang, D. Wu, Y. Hu, J. Li, S. Zhu, and M. Xiao, Nat. Photonics **12**, 596 (2018).
39. J. W. Goodman and M. E. Cox, *Introduction to Fourier Optics* (McGraw-Hill, 1968).
40. A. W. Lohmann and D. P. Paris, Appl. Opt. **6**, 1739 (1967).
41. T.-C. Poon and J.-P. Liu, *Introduction to Modern Digital Holography with MATLAB* (Cambridge University, 2014).
42. J. Imbrock, H. Hanafi, M. Ayoub, and C. Denz, Appl. Phys. Lett. **113**, 252901 (2018).
43. J.-G. Hua, F. Yu, Z.-N. Tian, Y.-H. Yu, and Y.-S. Yu, J. Laser Micro Nanoeng. **12**, 207 (2017).
44. W. Gandrud, IEEE J. Quantum Electron. **7**, 132 (1971).
45. N. Matsumoto, T. Ando, T. Inoue, Y. Ohtake, N. Fukuchi, and T. Hara, J. Opt. Soc. Am. A **25**, 1642 (2008).
46. M. M. Fejer, G. A. Magel, and E. J. Lim, Proc. SPIE **1148**, 213 (1990).
47. K. J. Wædegaard, H. D. Hansen, and P. Balling, Appl. Phys. B **113**, 345 (2013).